Architecture Optimization of a 3-DOF Translational Parallel Mechanism for Machining Applications, the Orthoglide

Damien Chablat, Philippe Wenger

Architecture Optimization of a 3-DOF Translational Parallel Mechanism for Machining Applications, the Orthoglide

Damien Chablat, Philippe Wenger (corresponding author)

***Abstract*— This paper addresses the architecture optimization of a 3-DOF translational parallel mechanism designed for machining applications. The design optimization is conducted on the basis of a prescribed Cartesian workspace with prescribed kinetostatic performances. The resulting machine, the Orthoglide, features three fixed parallel linear joints which are mounted orthogonally and a mobile platform which moves in the Cartesian x-y-z space with fixed orientation. The interesting features of the Orthoglide are a regular Cartesian workspace shape, uniform performances in all directions and good compactness. A small-scale prototype of the Orthoglide under development is presented at the end of this paper.**

***Index Terms*— Parallel mechanism, Optimal design, Singularity, Isotropic design, Workspace.**

I. INTRODUCTION

PARALLEL kinematic machines (PKM) are commonly claimed to offer several advantages over their serial counterparts, like high structural rigidity, high dynamic capacities and high accuracy [1], [2]. Thus, PKM are interesting alternative designs for high-speed machining applications.

This is why parallel kinematic machine-tools attract the interest of more and more researchers and companies. Since the first prototype presented in 1994 during the IMTS in Chicago by Gidding&Lewis (the VARIAX), many other prototypes have appeared.

However, the existing PKM suffer from two major drawbacks, namely, a complex workspace and highly non linear input/output relations. For most PKM, the Jacobian matrix which relates the joint rates to the output velocities is not constant and not isotropic. Consequently, the performances *e.g.* maximum speeds, forces, accuracy and rigidity) vary considerably for different points in the Cartesian workspace and for different directions at one given point. This is a serious drawback for machining applications [1], [3], [4]. To be of interest for machining applications, a PKM should preserve good workspace properties, that is, regular shape and acceptable kinetostatic performances throughout. In milling applications, the machining conditions must remain constant along the whole tool path [5]. In many research papers, this criterion is not taken into account in the algorithmic methods used for the optimization of the workspace volume [6], [7].

Most industrial 3-axis machine-tools have a serial kinematic architecture with orthogonal linear joint axes along the x, y and z directions. Thus, the motion of the tool in any of these directions is linearly related to the motion of one of the three actuated axes. Also, the performances are constant throughout the Cartesian workspace, which is a parallelepiped. The main drawback is inherent to the serial arrangement of the links, namely, poor dynamic performances. The purpose of this paper is to design a translational 3-axis PKM with the advantages of serial machine tools but without their drawbacks. Starting from a Delta-type architecture with three fixed linear joints and three articulated parallelograms, an optimization procedure is conducted in which two criteria are used successively, (i) the conditioning of the Jacobian matrix of the PKM [8], [9], [10], [11] and (ii) the manipulability ellipsoid [12]. The first criterion leads to an isotropic architecture that features a configuration where the tool forces and velocities are equal in all directions. The second criterion makes it possible to define the actuated joint limits and the link lengths with respect to a desired Cartesian workspace size and prescribed limits on the transmission factors. The resulting PKM, the Orthoglide, has a Cartesian workspace shape that is close to a cube whose sides are parallel to the planes xy, yz and xz respectively. A systematic design procedure is proposed to define the geometric parameters as function of the size of a prescribed cubic Cartesian workspace and bounded velocity and force transmission factors throughout.

Next section presents the existing PKM. The design parameters and the kinematics of the mechanism to be optimized are reported in Section 3. Section 4 is devoted to the design procedure of the Orthoglide and the presentation of the prototype.

II. EXISTING PKM

Most existing PKM can be classified into two main families. The PKM of the first family have fixed foot points and variable length struts. These PKM are generally called "hexapods" when they have 6 degrees of freedom. Hexapods have a Stewart-Gough parallel kinematic architecture. Many prototypes and commercial hexapod PKM already exist like the VARIAX (Gidding&Lewis), the CMW300 (Compagnie Mécanique des Vosges), the TORNADO 2000 (Hexel), the MIKROMAT 6X (Mikromat/IWU), the hexapod OKUMA (Okuma), the hexapod G500 (GEODETIC). In this first family, we find also hybrid architectures with a 2-axis wrist mounted in series to a 3-DOF "tripod" positioning structure (*e.g.* the TRICEPT from Neos-Robotics [13]). Since many machining

Damien Chablat and Philippe Wenger are with the Institut de Recherche en Communications et Cybernétique de Nantes (IRCCyN), 1, rue de la Noë, 44321 Nantes, France, email: Philippe.Wenger@irccyn.ec-nantes.fr

tasks require only 3 translational degrees of freedom, several 3-axis translational PKM have been proposed. There are several ways to design such mechanisms [20], [14], [15], [16]. In the first family, we find the Tsai mechanism and its variants. In these mechanisms, the mobile platform is connected to the base by three extensible limbs with a special arrangement of the universal joints that restrains completely the orientation of the mobile platform [18], [19].

The PKM of the second family have fixed length struts with moveable foot points gliding on fixed linear joints. In this category we find the HEXAGLIDE (ETH Zürich) which features six parallel (also in the geometrical sense) and coplanar linear joints. The HexaM (Toyoda) is another example with three pairs of adjacent linear joints lying on a vertical cone [21]. A hybrid parallel/kinematic PKM with three inclined linear joints and a two-axis wrist is the GEORGE V (IFW Uni Hanover). Many 3-axis translational PKM belong to this second family and use an architecture close to the linear Delta robot originally designed by Reymond Clavel for pick-and-place operations [22]. In this architecture, three parallelograms are used to provide the moving platform with pure translations. The TRIGLIDE (Mikron) has three parallel linear joints in an horizontal plane. The LINAPOD and the INDEX V100 have three vertical (non coplanar) linear joints [23]. The Urane SX (Renault Automation) and the QUICKSTEP (Krause & Mauser) have with three non coplanar horizontal linear joints [24]. The aforementioned five machines have parallel linear joints. This feature provides these machines with high stiffness in the direction of the linear joints and poor stiffness in the orthogonal directions. Thus, these machines are more suitable for specialized operations like drilling, than for general machining tasks. The STAR mechanism has three horizontal linear joints intersecting at one point [14]. Isotropic conditions for the STAR mechanisms were studied in [25] but a special type of singularity was shown to occur at the isotropic configuration if one prescribes unitary transmission factors [26]. At this singularity (a so-called "RPM-IO-II singularity" in the classification of [27]), there is a loss of both input and output motions and, at the same time, a redundant passive motion of each leg occurs. Recently, one 3-DOF translational mechanism with gliding foot points was found in three separate works to be isotropic throughout the Cartesian workspace [15], [16], [17]. The mobile platform is connected to three orthogonal linear drives through three identical planar 3-revolute jointed serial chains. Full isotropy is clearly an outstanding property. On the other hand, bulky legs are required to assure stiffness because these legs are subject to bending.

PKM with fixed length struts and moveable foot points are interesting because the actuators are fixed and the moving masses are lower than in the hexapods and tripods.

III. Problem formulation

A. Design Parameters

The machine-tool we want to design is a spatial translational PKM dedicated to general 3-axis machining tasks with the following requirements, (i) a configuration should exist where the transmission factors are equal to one in all directions, like in a translational serial machine (ii) the Cartesian workspace shape should be close to a cube of prescribed size with regular performances throughout, (iii) the design should be symmetric and use simple joints to lower the manufacturing costs, (iv) the PKM should be intrinsically stiff and (v) the PKM should have fixed linear actuated joints to lower the moving masses. To meet the last requirement, we start with a PKM architecture of the second family *i.e.* with fixed linear joints. The use of three articulated parallelograms assembled in an over-constrained way is an interesting solution to comply with requirement (iv). Requirements (i) and (ii) will be satisfied in Section 4 by the isotropic conditions and limited transmission factors constraints. It will be shown that requirement (i) imposes that the three actuated linear joint must be orthogonal, hence the name "orthoglide". To fulfill requirement (iii), finally, the three legs should use only revolute joints and be identical.

Figure 1 shows the basic kinematic architecture of a PKM that complies with requirements (iii), (iv) and (v) and that we will optimize with respect to requirements (i) and (ii). For more simplicity, the figure shows the PKM with the optimized (*i.e.* orthogonal) linear joints arrangement.

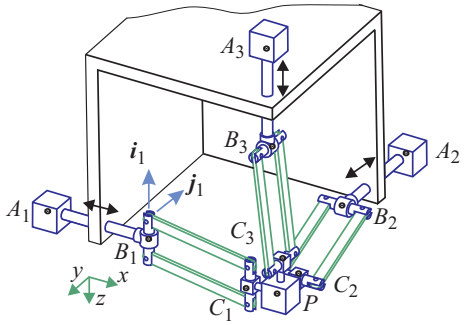

Fig. 1
BASIC KINEMATIC ARCHITECTURE

The linear joints can be actuated by means of linear motors or by conventional rotary motors with ball screws. Like in the Delta-type PKM, the output body is connected to the linear joints through a set of three parallelograms of equal lengths $L = B_iC_i$, so that it can move only in translation. The three legs are $PRPaR$ identical chains, where P, R and Pa stands for Prismatic, Revolute and Parallelogram joint, respectively. Thus, the mechanism is over-constrained. The arrangement of the joints in the $PRPaR$ chains have been defined to eliminate any special singularity [26]. Each base point A_i is fixed on the i^{th} linear axis such that $A_1A_2 = A_1A_3 = A_2A_3$. The points B_i and C_i are located on the i^{th} parallelogram as shown in Fig. 2.

The design parameters to be optimized are the parallelogram length, the position and orientation of each linear actuated joint axis and the range of the linear actuators.

B. Kinematic Equations and Singular configurations

Let θ_i and β_i denote the joint angles of the parallelogram about the axes $\mathbf{i}_i$ and $\mathbf{j}_i$, respectively (Fig. 2). Let ρ_1, ρ_2, ρ_3 denote the linear joint variables, $\rho_i = A_iB_i$.

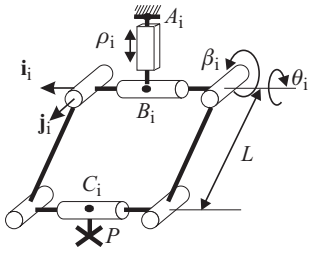

Fig. 2
LEG KINEMATICS

Let $\dot{\boldsymbol{\rho}}$ be referred to as the vector of actuated joint rates and $\dot{\mathbf{p}}$ as the velocity vector of point P:

$$\dot{\boldsymbol{\rho}} = [\dot{\rho}_1 \ \dot{\rho}_2 \ \dot{\rho}_3]^T, \quad \dot{\mathbf{p}} = [\dot{x} \ \dot{y} \ \dot{z}]^T$$

$\dot{\mathbf{p}}$ can be written in three different ways by traversing the three chains $A_iB_iC_iP$:

$$\dot{\mathbf{p}} = \mathbf{n}_i\dot{\rho}_i + (\dot{\theta}_i\mathbf{i}_i + \dot{\beta}_i\mathbf{j}_i) \times (\mathbf{c}_i - \mathbf{b}_i) \tag{1}$$

where $\mathbf{b}_i$ and $\mathbf{c}_i$ are the position vectors, in a given reference frame, of the points B_i and C_i, respectively, and $\mathbf{n}_i$ is the direction vector of the linear joints, for $i = 1, 2, 3$.

We want to eliminate the two passive joint rates $\dot{\theta}_i$ and $\dot{\beta}_i$ from Eqs. (1), which we do upon dot-multiplying Eqs. (1) by $\mathbf{c}_i - \mathbf{b}_i$:

$$(\mathbf{c}_i - \mathbf{b}_i)^T\dot{\mathbf{p}} = (\mathbf{c}_i - \mathbf{b}_i)^T\mathbf{n}_i\dot{\rho}_i \tag{2}$$

Equations (2) can now be cast in vector form, namely

$$\mathbf{A}\dot{\mathbf{p}} = \mathbf{B}\dot{\boldsymbol{\rho}}$$

where $\mathbf{A}$ and $\mathbf{B}$ are the parallel and serial Jacobian matrices, respectively:

$$\mathbf{A} = \begin{bmatrix} (\mathbf{c}_1 - \mathbf{b}_1)^T \\ (\mathbf{c}_2 - \mathbf{b}_2)^T \\ (\mathbf{c}_3 - \mathbf{b}_3)^T \end{bmatrix} \tag{3a}$$

$$\mathbf{B} = \begin{bmatrix} \eta_1 & 0 & 0 \\ 0 & \eta_2 & 0 \\ 0 & 0 & \eta_3 \end{bmatrix} \tag{3b}$$

with $\eta_i = (\mathbf{c}_i - \mathbf{b}_i)^T\mathbf{n}_i$ for $i = 1, 2, 3$.

The parallel singularities occur when the determinant of the matrix $\mathbf{A}$ vanishes, *i.e.* when $\det(\mathbf{A}) = 0$. In such configurations, it is possible to move locally the mobile platform whereas the actuated joints are locked. These singularities are particularly undesirable because the structure cannot resist any force. Equation (3a) shows that the parallel singularities occur when the three vectors $\mathbf{c}_i - \mathbf{b}_i$ are linearly dependent, that is when the pairs of points (B_i, C_i) lie in parallel planes (Fig. 3). To interpret this singularity, it is more convenient to regard the points C_i as coincident (this does not change the analysis since each offset C_iP can be included in ρ_i). Then, a parallel singularity occurs when the points B_1, B_2, B_3 and $C = C_1 = C_2 = C_3 = P$ are coplanar. Since, at a parallel singular configuration, P is always equally distant from B_1, B_2 and B_3, P is at the center of a circle of radius L that cuts the x, y and z axes at B_1, B_2 and B_3, respectively, where x, y and z are parallel to the three linear actuated joints, respectively (Fig. 3). The parallel singularities are defined by the surface generated by P when this circle "glides" along the x, y and z axes. A particular parallel singularity occurs when the links B_iC_i are parallel. The surface generated is a sphere of radius L and centered at the intersection of the x, y and z axes (Fig. 4).

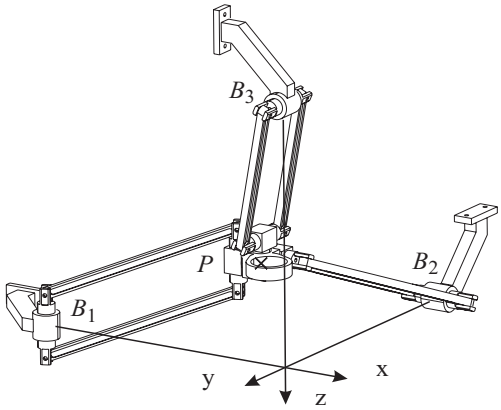

Fig. 3
PARALLEL SINGULAR CONFIGURATION IN THE GENERAL CASE

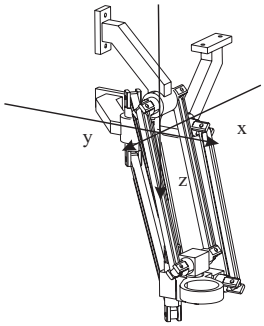

Fig. 4
PARALLEL SINGULAR CONFIGURATION WHEN B_iC_i ARE PARALLEL

Serial singularities arise when the serial Jacobian matrix $\mathbf{B}$ is no longer invertible *i.e.* when $\det(\mathbf{B}) = 0$. At a serial singularity a direction exists along which any Cartesian velocity cannot be produced. Eq. (3b) shows that $\det(\mathbf{B}) = 0$ when for one leg i, $(\mathbf{b}_i - \mathbf{a}_i) \perp (\mathbf{c}_i - \mathbf{b}_i)$, where $\mathbf{a}_i$ is the position vector of A_i. Thus, the serial singularities form three planes orthogonal to the x, y and z axis, respectively.

It will be shown in Section IV-D that the optimization of the Orthoglide puts the serial and parallel singularities far away from the Cartesian workspace. Also, even if the direct and inverse kinematics may theoretically have several solutions, only one solution exists in the Cartesian workspace [28].

IV. OPTIMIZATION OF THE DESIGN PARAMETERS

The aim of this section is to define the geometric parameters of the Orthoglide as a function of the size of a prescribed cubic

Cartesian workspace with bounded transmission factors. We first show that the orthogonal arrangement of the linear joints is imposed by the condition on the isotropy and manipulability: we want the Orthoglide to have an isotropic configuration with velocity and force transmission factors equal to one. Then, we impose that the transmission factors remain under prescribed bounds throughout the prescribed Cartesian workspace and we deduce the link dimensions and the joint limits. Limiting the force and velocity transmission factors makes it possible to guarantee a minimal kinematic stiffness throughout the Cartesian workspace. The structural stiffness (*i.e.* including the stiffness of all rods) is guaranteed by the over-constrained design and preliminary rods stiffness analyses [2]. A more detailed study of the Othoglide structural stiffness is currently conducted at IRCCyN with finite element analyses.

A. Condition Number and Isotropic Configuration

The Jacobian matrix is said to be isotropic when its condition number attains its minimum value of one [28]. The condition number of the Jacobian matrix is an interesting performance index which characterises the distortion of a unit ball under the transformation represented by the Jacobian matrix. The Jacobian matrix of a manipulator is used to relate (i) the joint rates and the Cartesian velocities, and (ii) the static load on the output link and the joint torques or forces. Thus, the condition number of the Jacobian matrix can be used to measure the uniformity of the distribution of the tool velocities and forces in the Cartesian workspace.

B. Isotropic Configuration of the Orthoglide

For parallel manipulators, it is more convenient to study the conditioning of the Jacobian matrix that is related to the inverse transformation, $\mathbf{J}^{-1}$. When $\mathbf{B}$ is not singular, $\mathbf{J}^{-1}$ is defined by:

$$\dot{\boldsymbol{\rho}} = \mathbf{J}^{-1}\dot{\mathbf{p}} \quad \text{with} \quad \mathbf{J}^{-1} = \mathbf{B}^{-1}\mathbf{A}$$

Thus:

$$\mathbf{J}^{-1} = \begin{bmatrix} (1/\eta_1)(\mathbf{c}_1 - \mathbf{b}_1)^T \\ (1/\eta_2)(\mathbf{c}_2 - \mathbf{b}_2)^T \\ (1/\eta_3)(\mathbf{c}_3 - \mathbf{b}_3)^T \end{bmatrix} \tag{4}$$

with $\eta_i = (\mathbf{c}_i - \mathbf{b}_i)^T\mathbf{n}_i$ for $i = 1, 2, 3$.

The matrix $\mathbf{J}^{-1}$ is isotropic when $\mathbf{J}^{-1}\mathbf{J}^{-T} = \sigma^2\mathbf{1}_{3\times3}$, where $\mathbf{1}_{3\times3}$ is the 3×3 identity matrix. Thus, we must have,

$$\frac{1}{\eta_1}||\mathbf{c}_1 - \mathbf{b}_1|| = \frac{1}{\eta_2}||\mathbf{c}_2 - \mathbf{b}_2|| = \frac{1}{\eta_3}||\mathbf{c}_3 - \mathbf{b}_3|| \tag{5a}$$

$$(\mathbf{c}_1 - \mathbf{b}_1)^T(\mathbf{c}_2 - \mathbf{b}_2) = 0 \tag{5b}$$

$$(\mathbf{c}_2 - \mathbf{b}_2)^T(\mathbf{c}_3 - \mathbf{b}_3) = 0 \tag{5c}$$

$$(\mathbf{c}_3 - \mathbf{b}_3)^T(\mathbf{c}_1 - \mathbf{b}_1) = 0 \tag{5d}$$

Equation (5a) states that the angle between the axis of the linear joint and the link B_iC_i must be the same for each leg i. Equations (5b–d) mean that the links B_iC_i must be orthogonal to each other. Figure 5 shows the isotropic configuration of the Orthoglide. Note that the orthogonal arrangement of the linear joints is not a consequence of the isotropy condition, but it stems from the condition on the transmission factors at the isotropic configuration, as shown in the next section.

C. Transmission factors

For serial 3-axis machine tools, a motion of an actuated joint yields the same motion of the tool (the transmission factors are equal to one). For parallel machines, these motions are generally not equivalent. When the mechanism is close to a parallel singularity, a small joint rate can generate a large velocity of the tool. This means that the positioning accuracy of the tool is lower in some directions for some configurations close to parallel singularities because the encoder resolution is amplified. In addition, a velocity amplification in one direction is equivalent to a loss of stiffness in this direction.

The manipulability ellipsoids of the Jacobian matrix of robotic manipulators was defined two decades ago [9]. This concept has then been applied as a performance index to parallel manipulators [3]. Note that, although the concept of manipulability is close to the concept of condition number, they do not provide the same information. The condition number quantifies the proximity to an isotropic configuration, *i.e.* where the manipulability ellipsoid is a sphere, or, in other words, where the transmission factors are the same in all the directions, but it does not inform about the value of the transmission factor.

The manipulability ellipsoid of $\mathbf{J}^{-1}$ is used here for (i) defining the orientation of the linear joints and (ii) defining the joint limits of the Orthoglide such that the transmission factors are bounded in the prescribed Cartesian workspace.

We want the transmission factors to be equal to one at the isotropic configuration like for a serial machine tool. This condition implies that the three terms of Eq. (5a) must be equal to one:

$$\frac{1}{\eta_1}||\mathbf{c}_1 - \mathbf{b}_1|| = \frac{1}{\eta_2}||\mathbf{c}_2 - \mathbf{b}_2|| = \frac{1}{\eta_3}||\mathbf{c}_3 - \mathbf{b}_3|| = 1 \tag{6}$$

which implies that $(\mathbf{b}_i - \mathbf{a}_i)$ and $(\mathbf{c}_i - \mathbf{b}_i)$ must be collinear for each i.

Since, at this isotropic configuration, links B_iC_i are orthogonal, Eq. (6) implies that the links A_iB_i are orthogonal, *i.e.* the linear joints are orthogonal. For joint rates belonging to a unit ball, namely, $||\dot{\boldsymbol{\rho}}|| \leq 1$, the Cartesian velocities belong to an ellipsoid such that:

$$\dot{\boldsymbol{p}}^T(\mathbf{J}\mathbf{J}^T)\dot{\boldsymbol{p}} \leq 1$$

The eigenvectors of matrix $(\mathbf{J}\mathbf{J}^T)^{-1}$ define the direction of its principal axes of this ellipsoid and the square roots ξ_1, ξ_2 and ξ_3 of the eigenvalues of $(\mathbf{J}\mathbf{J}^T)^{-1}$ are the lengths of the aforementioned principal axes. The velocity transmission factors in the directions of the principal axes are defined by $\psi_1 = 1/\xi_1$, $\psi_2 = 1/\xi_2$ and $\psi_3 = 1/\xi_3$. To limit the variations of this factor, we impose

$$\psi_{min} \leq \psi_i \leq \psi_{max} \tag{7}$$

throughout the Cartesian workspace. This condition determines the link lengths and the linear joint limits. To simplify the problem, we set $\psi_{min} = 1/\psi_{max}$.

D. Design of the Orthoglide for a Prescribed Cartesian Workspace

For usual machine tools, the Cartesian workspace is generally given as a function of the size of a right-angled parallelepiped. Due to the symmetrical architecture of the Orthoglide, the Cartesian workspace has a fairly regular shape. In fact, the workspace is defined by the intersection of three orthogonal cylinders topped with spheres. As shown in Fig. 5, it is easy to include a cube whose sides are parallel to the planes xy, yz and xz respectively. The aim of this section is

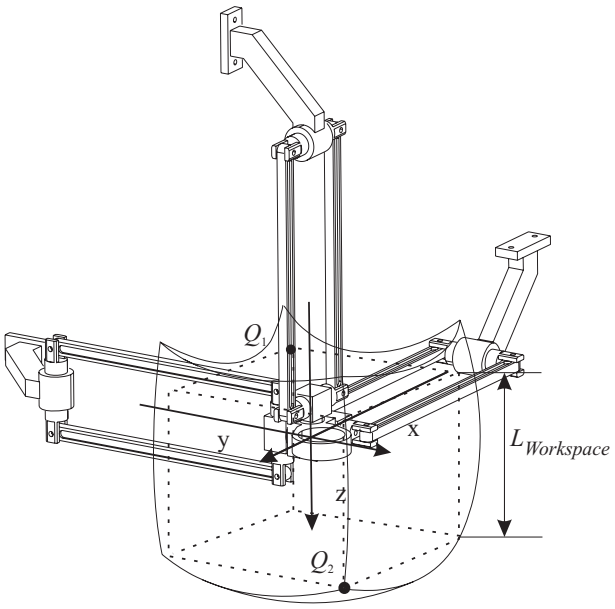

Fig. 5
ISOTROPIC CONFIGURATION AND CARTESIAN WORKSPACE OF THE ORTHOGLIDE MECHANISM AND POINTS Q_1 AND Q_2

to define the position of the base point A_i, the link lengths L and the linear actuator range $\Delta\rho$ with respect to the limits on the transmission factors defined in Eq. (7) and as a function of the size of the prescribed Cartesian workspace $L_{Workspace}$.

The proposed optimization scheme is divided into three steps.

1) First, two points Q_1 and Q_2 are determined in the prescribed cubic Cartesian workspace (Fig. 5) such that if the transmission factor bounds are satisfied at these points, they are satisfied in all the prescribed Cartesian workspace.
2) The points Q_1 and Q_2 are used to define the leg length L as function of the size of the prescribed cubic Cartesian workspace.
3) Finally, the positions of the base points A_i and the linear actuator range $\Delta\rho$ are calculated such that the prescribed cubic Cartesian workspace is fully included in the Cartesian workspace of the Orthoglide.

Step 1: The transmission factors are equal to one at the isotropic configuration. These factors increase or decrease when the tool center point moves away from the isotropic configuration and they tend towards zero or infinity in the vicinity of the singularity surfaces. It turns out that the points Q_1 and Q_2 defined at the intersection of the Cartesian workspace boundary with the axis $x = y = z$ (in a reference frame (O, x, y, z) centered at the intersection of the three linear joint axes, Fig. 5) are the closest ones to the singularity surfaces, as illustrated in Fig. 6 which shows on the same top view the Orthoglide in the two parallel singular configurations of figures 3 and 4. Thus, we may postulate the intuitive result that if the prescribed bounds on the transmission factors are satisfied at Q_1 and Q_2, then these bounds are satisfied throughout the prescribed cubic Cartesian workspace. In fact, this result can be proved using interval analysis [29].

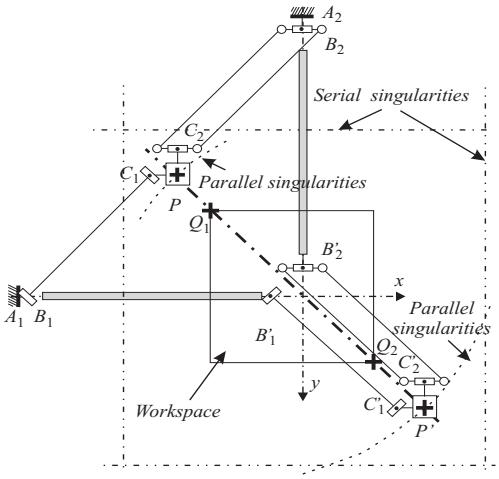

Fig. 6
POINTS Q_1 AND Q_2 AND THE SINGULAR CONFIGURATIONS (TOP VIEW)

Step 2: At the isotropic configuration, the angles θ_i and β_i are equal to zero by definition. When the tool center point P is at Q_1, $\rho_1 = \rho_2 = \rho_3 = \rho_{min}$ (Fig. 7). When P is at Q_2, $\rho_1 = \rho_2 = \rho_3 = \rho_{max}$ (Fig. 8).

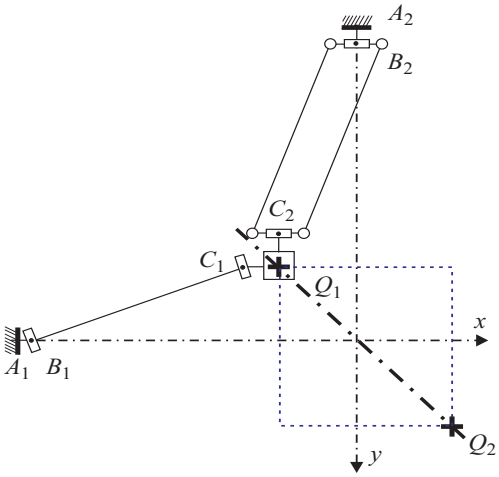

Fig. 7
Q_1 CONFIGURATION

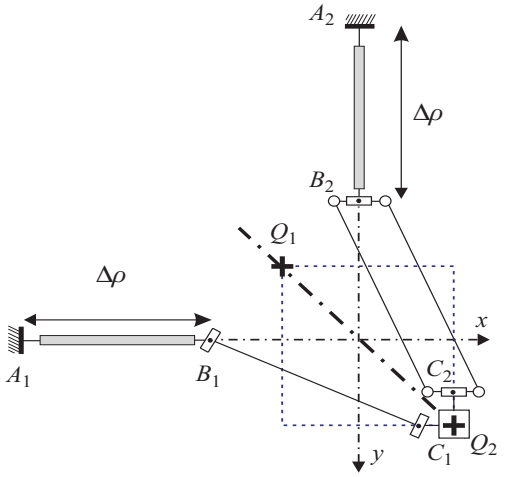

Fig. 8
Q_2 CONFIGURATION

We pose $\rho_{min} = 0$ for more simplicity.

The position of P along the z axis can be written equivalently as $z = -\sin(\beta_1)L$ and $z = \sin(\theta_2)\cos(\beta_2)L$ by traversing the two chains $A_1B_1C_2P$ and $A_2B_2C_2P$, respectively. On the axis (Q_1Q_2), $\beta_1 = \beta_2 = \beta_3$ and $\theta_1 = \theta_2 = \theta_3$. We note,

$$\beta_1 = \beta_2 = \beta_3 = \beta \quad \text{and} \quad \theta_1 = \theta_2 = \theta_3 = \theta \tag{8}$$

Thus, the angle β can be written as a function of θ,

$$\beta = -\arctan(\sin(\theta)) \tag{9}$$

Finally, by substituting Eq. (9) into Eq. (4), the inverse Jacobian matrix $\mathbf{J}^{-1}$ can be simplified as follows

$$\mathbf{J}^{-1} = \begin{bmatrix} 1 & -\tan(\theta) & -\tan(\theta) \\ -\tan(\theta) & 1 & -\tan(\theta) \\ -\tan(\theta) & -\tan(\theta) & 1 \end{bmatrix}$$

Thus, the square roots of the eigenvalues of $(\mathbf{J}\mathbf{J}^T)^{-1}$ are,

$$\xi_1 = |2\tan(\theta) - 1| \quad \text{and} \quad \xi_2 = \xi_3 = |\tan(\theta) + 1|$$

And the three velocity transmission factors are,

$$\psi_1 = \frac{1}{|2\tan(\theta) - 1|} \quad \text{and} \quad \psi_2 = \psi_3 = \frac{1}{|\tan(\theta) + 1|} \tag{10}$$

The joint limits on θ are located on both sides of the isotropic configuration. To calculate the joint limits, we solve the following inequations,

$$\frac{1}{\psi_{max}} \leq \frac{1}{|2\tan(\theta) - 1|} \leq \psi_{max} \tag{11a}$$

$$\frac{1}{\psi_{max}} \leq \frac{1}{|\tan(\theta) + 1|} \leq \psi_{max} \tag{11b}$$

where the value of ψ_{max} depends on the performance requirements. Two sets of joint limits ($[\theta_{Q_1}\ \beta_{Q_1}]$ and $[\theta_{Q_2}\ \beta_{Q_2}]$) are found in symbolic form. The detail of this calculation is given in the Appendix.

The position vectors $\mathbf{q}_1$ and $\mathbf{q}_2$ of the points Q_1 and Q_2, respectively, can be easily defined as a function of L (Figs. 7 and 8),

$$\mathbf{q}_1 = [q_1\ q_1\ q_1]^T \quad \text{and} \quad \mathbf{q}_2 = [q_2\ q_2\ q_2]^T \tag{12a}$$

with

$$q_1 = -\sin(\beta_{Q_1})L \quad \text{and} \quad q_2 = -\sin(\beta_{Q_2})L \tag{12b}$$

The size of the Cartesian workspace is,

$$L_{Workspace} = |q_2 - q_1|$$

Thus, L can be defined as a function of $L_{Workspace}$.

$$L = \frac{L_{Workspace}}{|\sin(\beta_{Q_2}) - \sin(\beta_{Q_1})|}$$

Step 3: We want to determine the positions of the base points, namely, $a = OA_1 = OA_2 = OA_3$. When the tool center point P is at Q_1' defined as the projection onto the y axis of Q_1, $\rho_2 = 0$ and, (Fig. 9)

$$OA_2 = OQ_1' + Q_1'C_2 + C_2A_2$$

Since $\rho_2 = 0$, $C_2A_2 = C_2B_2 = L$. With $OA_2 = a$, $Q_1'C_2 = PC_2 = -e$ and $OQ_1' = q_1$, we get,

$$a = q_1 - e - L$$

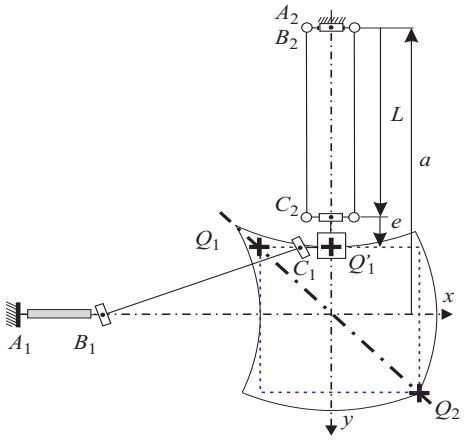

Fig. 9
THE POINT Q_1' USED FOR THE DETERMINATION OF a

Since q_1 is known from Eqs. (12a) and (17b), a can be calculated as function of e, L and ψ_{max}.

Now, we have to calculate the linear joint range $\Delta\rho = \rho_{max}$ (we have posed ρ_{min}=0).

When the tool center point P is at Q_2, $\rho = \rho_{max}$. Projecting $A_2P = A_2B_2 + B_2C_2 + C_2P$ on the y axis yields,

$$\rho_{max} = q_2 - a - \cos(\theta_{Q_2})\cos(\beta_{Q_2})L - e$$

E. Prototype

Using the aforementioned two kinetostatic criteria, a small-scale prototype has been constructed in our laboratory (Figure 10). The three parts (1), (2) and (3) have been designed to prevent each parallelogram from colliding with the corresponding linear motion guide. Also, the shifted position of the tool center point P limits the collisions between the parallelograms and the workpiece. The actuated joints used

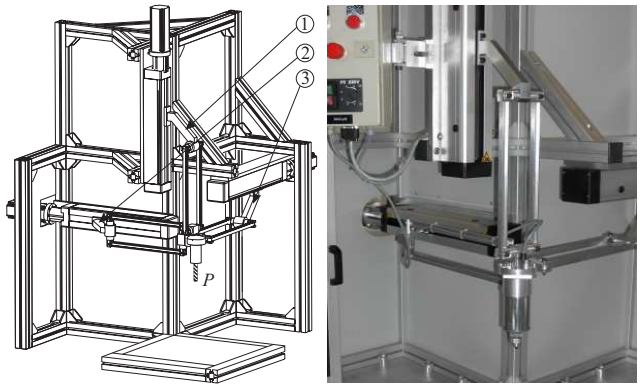

Fig. 10
CATIA MODEL OF THE ORTHOGLIDE (LEFT) AND PROTOTYPE (RIGHT)

for this prototype are rotary motors with ball screws. The prescribed performances of the Orthoglide prototype are a Cartesian velocity of $1.2m/s$ and an acceleration of $14m/s^2$ at the isotropic point. The desired payload is $4kg$. The size of its prescribed cubic Cartesian workspace is $200 \times 200 \times 200\ mm$. We limit the variations of the velocity transmission factors as,

$$1/2 \leq \psi_i \leq 2 \tag{13}$$

The resulting length of the three parallelograms is $L = 310\ mm$ and the resulting range of the linear joints is $\Delta\ \rho = 257\ mm$. Thus, the ratio of the range of the actuated joints to the size of the prescribed Cartesian workspace is $r = 200/257 = 0.78$. This ratio is high compared to other PKM. The three velocity transmission factors are depicted in Fig. 11. These factors are given in a z-cross section of the Cartesian workspace passing through Q_1.

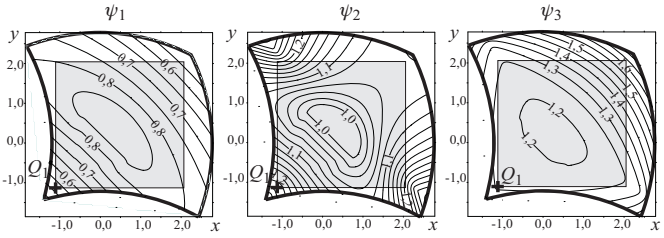

Fig. 11
THE THREE VELOCITY TRANSMISSION FACTORS IN A z-CROSS SECTION OF THE CARTESIAN WORKSPACE PASSING THROUGH Q_1

V. CONCLUSIONS

The Orthoglide is a new Delta-type PKM dedicated to 3-axis rapid machining applications that was designed to meet the advantages of both serial 3-axis machines (regular workspace and homogeneous performances) and parallel kinematic architectures (good dynamic performances). A systematic procedure has been provided to define the geometric parameters of the Orthoglide as functions of the size of a prescribed cubic Cartesian workspace and bounded velocity and force transmission factors.

The Orthoglide has been designed under isotropic conditions and limited transmission factors. Low inertia and intrinsic stiffness have been set as additional design requirements. Thus, three articulated parallelograms have been used, rather than legs subject to bending as in the fully isotropic mechanisms proposed in [15], [16], [17]. At the isotropic configuration, a displacement of a linear joint yields the same displacement of the tool in the corresponding Cartesian direction like in a serial machine. The Cartesian workspace is simple, regular and free of singularities and self-collisions. It is fairly regular and the performances are homogeneous throughout the Cartesian workspace. Thus, the entire Cartesian workspace is really available for tool paths. These features make the Orthoglide a novel design as compared to the existing Delta-type PKM structures. A small-scale prototype Orthoglide has been built at IRCCyN to demonstrate the feasibility of the design. Dynamic model based control laws will be implemented [30] and first machining experiments with plastic parts will be conducted.

ACKNOWLEDGMENTS

This works is supported by Région Pays-de-Loire, Agence Nationale pour la Valorisation de la Recherche, École des Mines de Nantes and C.N.R.S.

S. Bellavoir, G. Branchu, P. Lemoine and P. Molina are gratefully acknowledged for their technical help.

REFERENCES

[1] Tlusty, J., Ziegert, J, and Ridgeway, S., 1999, "Fundamental Comparison of the Use of Serial and Parallel Kinematics for Machine Tools," Annals of the CIRP, Vol. 48:1, pp. 351–356.
[2] Wenger, P., Gosselin, C. and Maille, B., 1999, "A Comparative Study of Serial and Parallel Mechanism Topologies for Machine Tools," Proc. PKM'99, Milano, pp. 23–32.
[3] Kim, J., Park, C., Kim, J. and Park F.C., 1997, "Performance Analysis of Parallel Manipulator Architectures for CNC Machining Applications," Proc. IMECE Symp. On Machine Tools, Dallas.
[4] Wenger, P., Gosselin, C. and Chablat, D., 2001, "A Comparative Study of Parallel Kinematic Architectures for Machining Applications," Proc. Workshop on Computational Kinematics, Seoul, Korea, pp. 249–258.
[5] Rehsteiner, F., Neugebauer, R., Spiewak, S. and Wieland, F., 1999, "Putting Parallel Kinematics Machines (PKM) to Productive Work," Annals of the CIRP, Vol. 48:1, pp. 345–350.
[6] Luh, C-M., Adkins, F.A., Haug, E.J. and Qui, C.C., 1996, "Working Capability Analysis of Stewart platforms," Transactions of ASME, pp. 220–227.
[7] Merlet, J-P., 1999, "Dertemination of 6D Workspace of Gough-Type Parallel Manipulator and Comparison between Different Geometries," The Int. Journal of Robotic Research, Vol. 19, No. 9, pp. 902–916.
[8] Golub, G. H. and Van Loan, C. F., Matrix Computations, The John Hopkins University Press, Baltimore, 1989.
[9] Salisbury, J-K. and Craig, J-J., 1982, "Articulated Hands: Force Control and Kinematic Issues," The Int. J. Robotics Res., Vol. 1, No. 1, pp. 4–17.
[10] Huang, T. and Whitehouse, D., 1998, "Local Dexterity, Optimal Architecture and Optimal Design of Parallel Machine Tools," Annals of the CIRP, Vol. 47:1, pp. 347–351.
[11] Zanganeh, K.E. and Angeles, J., "Kinematic isotropy and the optimum design of parallel manupilators," The Int. J. Robotics Res., Vol. 16, No. 2, pp. 185–197.
[12] Yoshikawa, T., 1985, "Manipulability of Robot Mechanisms," The Int. J. Robotics Res., Vol. 4, No. 2, pp. 3–9.
[13] Neumann, K.E., 1988, "Robot," United State Patent no. 4,732,625.
[14] Hervé, J.M. and Sparacino, F., 1991, "Structural Synthesis of Parallel Robots Generating Spatial Translation," 5th Int. Conf. on Adv. Robotics, IEEE n 91TH0367-4, Vol. 1, pp. 808–813.

[15] Carricato, M., Parenti-Castelli, V., 2002, "Singularity-free fully isotropic translational parallel manipulators," The Int. J. Robotics Res., Vol. 21, No. 2, pp. 161–174.

[16] Kong, X. and Gosselin, C.M., 2002, "Type synthesis of linear translational parallel manipulators," in Lenarčič, J. and Thomas, F. (editors), *Advances in Robot Kinematic*, Kluwer Academic Publishers, June, pp. 453–462.

[17] Kim, H.S. and Tsai, L.W., 2002, "Evaluation of a Cartesian manipulator," in Lenarčič, J. and Thomas, F. (editors), *Advances in Robot Kinematic*, Kluwer Academic Publishers, June, pp. 21–38.

[18] Tsai, L.W. and Joshi, S., 2000, "Kinematics and Optimization of a Spatial 3-UPU Parallel Manipulator," ASME Journal of Mechanical Design, Vol. 122, pp. 439–446.

[19] Di Gregorio, R. and Parenti-Castelli, V., 1998, "A Translational 3-DOF Parallel Manipulator," in Lenarčič, J. and Husty, M. (editors), *Advances in Robot Kinematic*, Kluwer Academic Publishers, June, pp. 49–58.

[20] Reboulet, C. and Lambert, C., 1990, "Dispositif manipulateur pour déplacer un objet dans l'espace parallèlement à lui-même," French Patent no. 90.15.846.

[21] Toyama, T. et al, 1998, "Machine Tool Having Parallel Structure," United State Patent no. 5,715,729.

[22] Clavel, R., 1988, "DELTA, a fast robot with parallel geometry," Proceedings of the 18th International Symposium of Robotic Manipulators, IFR Publication, pp. 91–100.

[23] Pritschow, G. and Wurst, K.H., 1997, "Systematic design of hexapods and other parallel link systems," Annals of CIRP, Vol 46:1, pp. 541–548.

[24] Company, O., Pierrot, F., Launay, F. and Fioroni, C., 2000, "Modelling and Preliminary Design Issues of a 3-axis Parallel Machine-Tool," Int. Conf. on PKM 2000, Ann Arbor, USA, pp. 14–23.

[25] Baron, L. and Bernier G., 2001, "The Design of Parallel Manipulators of Star Topology under Isotropic Constraint," Proc. DETC ASME, Pittsburg, Pennsylvania, USA.

[26] Majou F., Wenger, P. and Chablat, D., 2002, "Design of a 3-Axis Parallel Machine Tool for High Speed Machining: The Orthoglide," 4^{th} Int. Conf. on Integrated Design and Manufacturing in Mechanical Engineering, Clermont-Ferrand, France. D. Zlatanov, R.

[27] Zlatanov, D., Fenton, G. and Benhabib, B., 1994, "Singularity analysis of mechanism and Robots via a Velocity Equation Model of the Instantaneous Kinematics," Proc. IEEE Int. Conf. on Rob. and Aut., San Diego, U.S.A., pp. 986–991.

[28] Wenger, P. and Chablat, D., 2000, "Kinematic Analysis of a new Parallel Machine Tool: the Orthoglide," in Lenarčič, J. and Stanišić, M.M. (editors), *Advances in Robot Kinematic*, Kluwer Academic Publishers, June, pp. 305–314.

[29] Chablat, D., Wenger, P. and Merlet, J.P., 2002, "Workspace Analysis of the Orthoglide using Interval Analysis," in Lenarčič, J. and Thomas, F. (editors), *Advances in Robot Kinematic*, Kluwer Academic Publishers, June, pp. 397–406.

[30] Guegan, S. and Khalil, W., 2002, "Dynamic modeling of the Orthoglide," in Lenarčič, J. and Thomas, F. (editors), *Advances in Robot Kinematic*, Kluwer Academic Publishers, June, pp. 387–396.

VI. Appendix

To calculate the joint limits on θ and β, we solve the followings inequations, from the Eqs. 11,

$$|2\tan(\theta)-1| \leq \psi_{max} \quad \frac{1}{|2\tan(\theta)-1|} \leq \psi_{max} \tag{14}$$

Thus, we note,

$$f_1 = |2\tan(\theta)-1| \quad f_2 = 1/|2\tan(\theta)-1| \tag{15}$$

Fig. (12) shows f_1 and f_2 as function of θ along (Q_1Q_2). The four roots of $f_1 = f_2$ in $[-\pi\ \pi]$ are,

$$s_1 = -\arctan\left((1+\sqrt{17})/4\right) \tag{16a}$$
$$s_2 = -\arctan\left(1/2\right) \tag{16b}$$
$$s_3 = 0 \tag{16c}$$
$$s_4 = \arctan\left((-1+\sqrt{17})/4\right) \tag{16d}$$

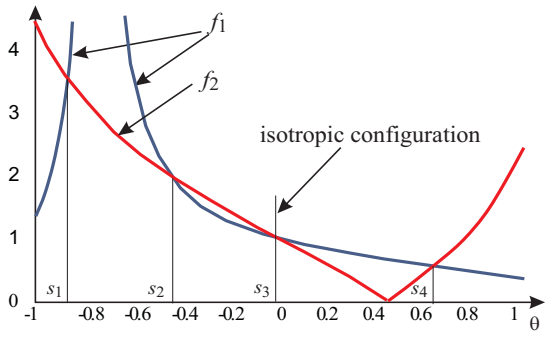

Fig. 12
f_1 AND f_2 AS FUNCTION OF θ ALONG (Q_1Q_2)

with

$$f_1(s_1) = (-3+\sqrt{17})/4 \quad f_1(s_2) = 2 \tag{16e}$$
$$f_1(s_3) = 1 \quad f_1(s_4) = (3+\sqrt{17})/4 \tag{16f}$$

The isotropic configuration is located at the configuration where $\theta = \beta = 0$. The limits on θ and β are in the vicinity of this configuration. Along the axis (Q_1Q_2), the angle θ is lower than 0 when it is close to Q_2, and greater than 0 when it is close to Q_1.

To find θ_{Q_1}, we study the functions f_1 and f_2 which are both decreasing on $[0\ \arctan(1/2)]$. Thus, we have,

$$\theta_{Q_1} = \arctan\left(\frac{\psi_{max}-1}{2\psi_{max}}\right) \tag{17a}$$
$$\beta_{Q_1} = -\arctan\left(\frac{\psi_{max}-1}{\sqrt{5\psi_{max}^2-2\psi_{max}+1}}\right) \tag{17b}$$

In the same way, to find θ_{Q_2}, we study the functions f_1 and f_2 on $[s_1\ 0]$. The three roots s_1, s_2 and s_3 define two intervals. If $\psi_{max} \in [f_1(s_1)\ f_1(s_2)]$, we have,

$$\theta_{Q_2} = -\arctan\left(\frac{\psi_{max}-1}{\psi_{max}}\right) \tag{18a}$$
$$\beta_{Q_2} = \arctan\left(\frac{\psi_{max}-1}{\sqrt{2\psi_{max}^2-2\psi_{max}+1}}\right) \tag{18b}$$

otherwise, if $\psi_{max} \in [f_1(s_2)\ f_1(s_3)]$,

$$\theta_{Q_2} = -\arctan\left(\frac{\psi_{max}-1}{2}\right) \tag{18c}$$
$$\beta_{Q_2} = \arctan\left(\frac{\psi_{max}-1}{\sqrt{{\psi_{max}}^2-2\psi_{max}+5}}\right) \tag{18d}$$